

# Computational Analysis of Hovering Hummingbird Flight

Zongxian Liang<sup>1</sup> and Haibo Dong<sup>2</sup>

*Department of Mechanical & Materials Engineering,  
Wright State University, Dayton, OH 45435*

Mingjun Wei<sup>3</sup>

*Department of Mechanical and Aerospace Engineering,  
New Mexico State University, Las Cruces, NM 88003*

Different from large-size birds, hummingbirds are found to share more common flight patterns with insects, especially in hovering motion. Comparing to hovering insects, hummingbird wing kinematics uses apparent asymmetric motions during downstroke and upstroke. In current study, we present a direct numerical simulation of modeled hummingbird wings undergoing hover flight (Tobalske et al. JEB 2007). 3D wake structures and associated aerodynamic performance are of particular interests in this paper. Computational results are also compared with PIV experiments (Warrick et al. 2005 ).

## NOMENCLATURE

$C_\phi$	The ratio of time of downstroke to a stroke
$\phi$	Stroke angle, deg
$\phi_m$	Azimuthal amplitude, deg
$\alpha_c$	Chord angle, deg
$\gamma$	Stroke plane angle relative to the horizontal plane, deg
$\beta$	Body angle, deg
$\eta$	Pitching angle, deg
$\theta$	Heaving angle, deg
$T$	Time of a whole wing stroke, sec
$\bar{U}$	Average tip speed, m/s
$c$	mean chord length, m
$C_L$	Force coefficient in y direction
$C_X$	Force coefficient in x direction
$C_Z$	Force coefficient in z direction

## Introduction

Being a small-scale bird, hummingbird is found to share more common flight patterns with insects (Weis-Fogh 1972) other than large-scale birds especially in hovering motion. The Reynolds number for hummingbird hover flight ranges from  $10^3$  to  $10^4$  (Altshuler et al. 2004) and flapping frequency is about 41Hz (Tobalske et al. 2007). Thus, hummingbird is widely thought to employ aerodynamic mechanisms similar to those used by insects in spite of the differences in

<sup>1</sup> Ph.D Student, liang.5@wright.edu .

<sup>2</sup> Assistant Professor, AIAA Senior Member, haibo.dong@wright.edu.

<sup>3</sup> Assistant Professor, AIAA Member, mjwei@nmsu.edu.

musculoskeletal system. Using particle image velocimetry (PIV) techniques, researchers have attempted to provide visual details into the essential of unsteady fluid dynamics of hummingbird (Warrick et al. 2005, Altshuler et al. 2009). It is found that hovering hummingbird produces 75% of total lift in downstroke and 25% in upstroke of wing motion. Whereas in insects hover flight, the lift is commonly found to be produced approximately evenly in both strokes (Dickinson et al. 1999). Moreover, leading-edge vortex (Ellington et al. 1996), which is observed in both downstroke and upstroke of insect hover flight (Dickinson et al. 1999, Sane and Dickinson 2001), however, is not seen either at the beginning or the end of the upstroke but seen in the full downstroke (Warrick et al. 2005). One explanation is that hummingbirds have higher angle of attack at mid-downstroke than during mid-upstroke and only have partially inversion of wing camber at distal portion of wing during upstroke (Warrick et al. 2005). However, it is still lack of comprehensive computational or experimental work to reveal the 3D unsteady vortex formations of this complicated motion.

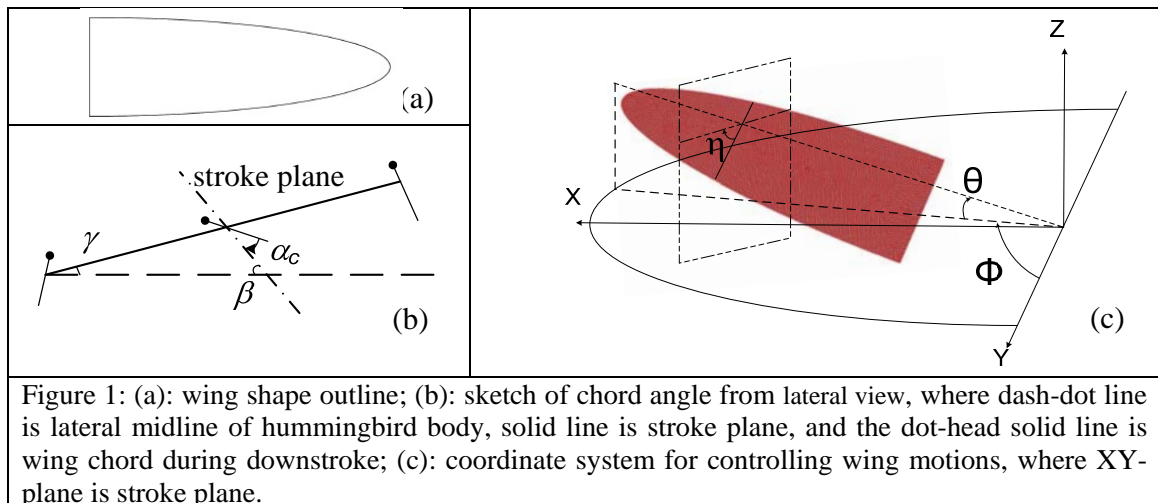
In this paper, we describe a direct numerical simulation of modeled hummingbird wings undergoing hover flight based on datum from Tobalske et al. 2007, to investigate the complete details of three-dimensional vortex topologies and associated aerodynamic performance. Results will also be compared with Warrick et al. 2005.

## Results

A second-order finite-difference based immersed-boundary solver (Dong et al. 2006, Mittal et al. 2008) has been developed which allows us to simulate flows with complex immersed 3-D moving bodies. The method employs a second-order central difference scheme in space and a second-order accurate fractional-step method for time advancement. Code validations and details of numerical methodologies can be found in Mittal et al. 2008.

In this section, a sequence of numerical simulations that explore the wake structures and associated aerodynamic performance of modeled hummingbird wings in hovering flight are presented. Model configuration and kinematics (Tobalske et al. 2007) approach are discussed first. Following this, the wake topology due to prescribed kinematics and aerodynamic force production are examined.

### A. Wing Configuration and Prescribed Wing Kinematics



A half elliptic wing analogical to hummingbird wing as shown in Figure 1(a) is employed

in this paper. Wing aspect-ratio is 9.1, which is comparable to average hummingbird wing aspect-ratio 9 (Tobalske et al. 2007). The pitching axis is through quarter chord and perpendicular to minor axis of the wing as shown in Figure 1(c).

Simplified kinematics described in Tobalske et al. 2007 for hover flight was implemented and controlled by the parameters in Figure 1(b) and 1(c). Especially, the stroke angle is defined as

$$\phi(t) = \begin{cases} \phi_m \cos\left(\frac{\pi t}{C_\phi T}\right) & \text{downstroke} \\ \phi_m \cos\left(\pi\left(\frac{t/T - C_\phi}{1 - C_\phi} + 1\right)\right) & \text{upstroke} \end{cases}$$

where  $\phi_m = 54.5^\circ$  is the azimuthal amplitude,  $C_\phi = 0.48$  is the ratio of the time spending in downstroke to that of a full stroke.

Following the definitions in Tobalske et al. 2007, stroke plane angle and body angle relative to the horizontal plane are  $\gamma$  and  $\beta$  (Figure 1), respectively. Chord angle ( $\alpha_c$ ) is reconstructed from the first eight terms of Fourier series of chord angle curve (Tobalske et al. 2007) in the form of

$$\alpha_c = \sum_{k=1}^8 a(k) \cos(2\pi kt) + b(k) \sin(2\pi kt)$$

Where  $a(k)$  and  $b(k)$  are Fourier coefficients. As shown in Figure 1(b), pitching angle in laboratory coordinate system is defined as  $\alpha_c + \gamma + \beta$ .

The Reynolds number was defined as  $Re = \bar{U}c/\nu$  (with average tip speed  $\bar{U}$ , mean chord length  $c$ , and kinematic viscosity  $\nu$  of the fluid). In the simulation,  $Re$  number is set to 3000. Strouhal number,  $St = fA/\bar{U}$  (Taylor et al. 2003), which is based on wingtip excursion  $A$  ( $A = b \sin \phi_m$ , where  $b$  is span), wing stroke frequency, and average tip speed, is 0.214 for this hover flight.

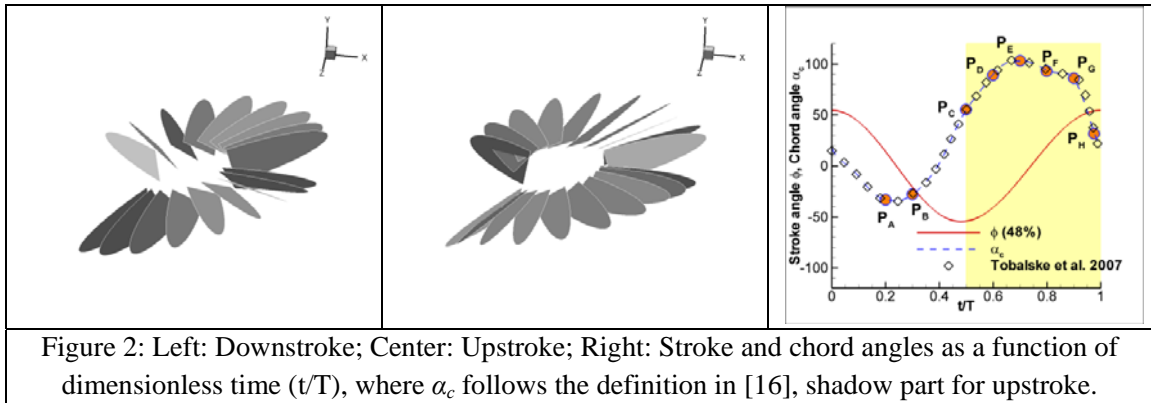
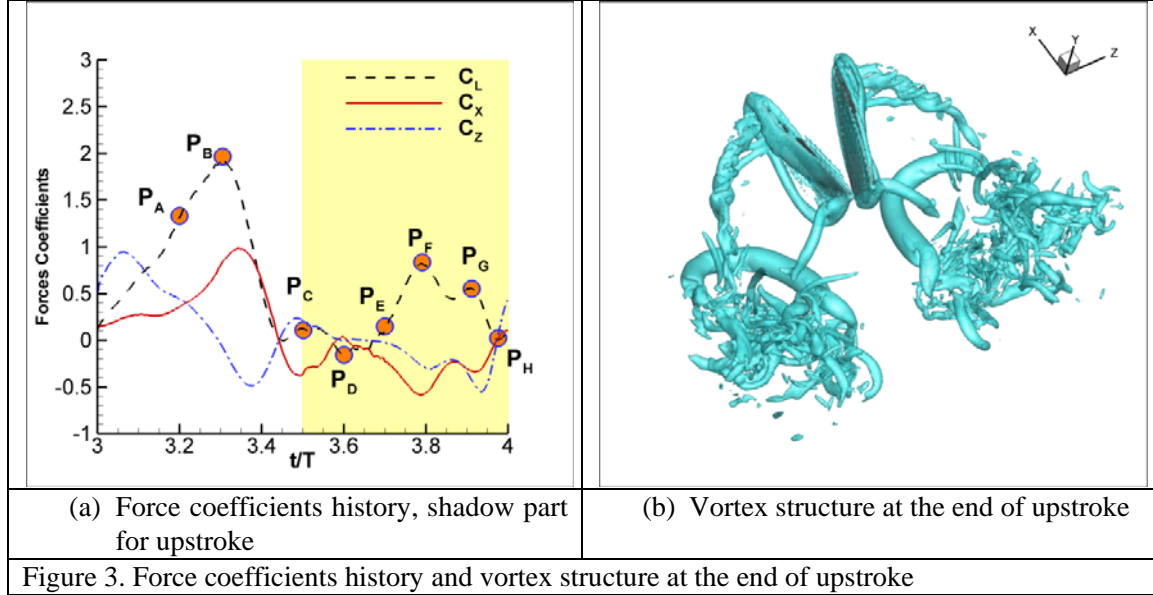


Figure 2: Left: Downstroke; Center: Upstroke; Right: Stroke and chord angles as a function of dimensionless time ( $t/T$ ), where  $\alpha_c$  follows the definition in [16], shadow part for upstroke.

The wingbeat begins with downstroke then upstroke. The downstroke is nearly sinusoidal shape (Figure 2), whereas the upstroke consists of initial pitching-down rotation with translational acceleration, followed by translation with chord angle gradually decreasing, and finally pitching-up rotation with translational deceleration. Based on domain independence studies and grid size independent studies, a domain size of  $30 \times 30 \times 30$  and a  $201 \times 121 \times 237$  grid has been finally chosen for all simulations.

## B. Analysis of 3D Flapping Flight



The force coefficients (defined by  $C = \frac{F}{(\frac{1}{2})\rho\bar{U}^2 S_{wing}}$ , where  $S_{wing}$  is the wing area and  $F$  is the force) history for the fourth cycle, at which the flow field is thought to be steady, is shown in Figure 3(a) and average forces in three directions for half-stroke and entire stroke are tabulated in Table 1. It can be found in Table 1 that the amount of lift generated during downstroke is 2.95 times of that generated during upstroke. This matches with the results of Warrick et al. 2005, which concluded that the amount of lift generation in downstroke is 3 times of that in upstroke for hummingbird hover flight. Moreover, the average lift is one order of magnitude larger than the average forces in other two directions.

Table 1: Comparison of  $C_L$ ,  $C_X$  and  $C_Z$  of right wing

	$C_L$	$C_X$	$C_Z$
<i>Downstroke</i>	0.932	0.387	0.273
<i>Upstroke</i>	0.316	-0.264	-0.120
<i>Total Avg.</i>	0.623	0.060	0.076

Figure 3(b) shows a 3-D perspective view of the wake topologies at the end of upstroke by using isosurfaces of the eigenvalue imaginary part of the velocity gradient tensor  $\frac{\partial u_i}{\partial x_j}$ . Two vortex rings, VR1, VR2 are circularly generated by trailing edge of the wing and the wing tip vortex during downstroke. These are similar to the discussion of Figure 9 in Altshuler et al. 2009. Strong downwash is expected to be induced by these two vertically oriented rings. Leading edge vortex (LEV), tip vortex (TPV), and trailing edge vortex (TV) are also clearly shown in the plot and connected to the vortex rings. In order to qualitatively understand the wake structures from computational results, we use two cross-section views to compare with the PIV results in Warrick et al. 2005.

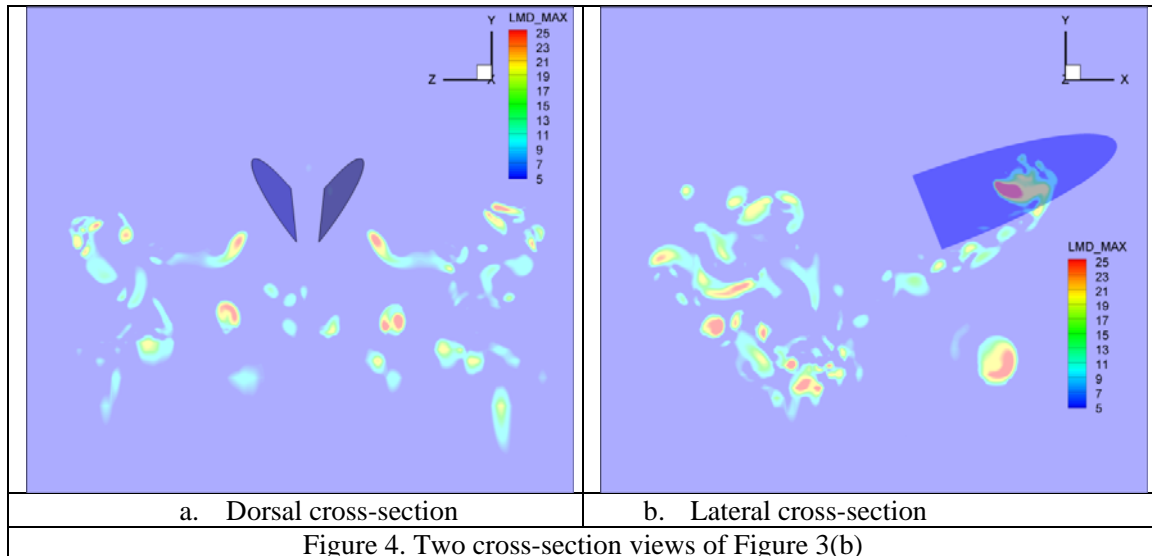


Figure 4. Two cross-section views of Figure 3(b)

Figure 4 shows two cross-sections of wake structures in Figure 3(b). Figure 4(a) is a slice cut in YZ-plane parallel to the X-axis near the root of wing and Figure 4(b) is a cross-section cut near the half-span length of wing. Comparing to Figure 2 in Warrick et al. 2005, vortices U1 and D1 in Figure 4(a) are in accordance with the vortices U and D in Warrick et al. 2005 respectively. Vortex U2 and D2 can also be found in Warrick et al. 2005. Here, vortices D1 and D2 form the downstroke vortex ring VR2 as seen in Figure 3(b). In Figure 4(b), both tip vortex (TPV) and slice of vortex ring VR2 can be found in the Figure 2 of Warrick et al. 2005.

To better understand how the leading edge vortex develops and sheds during the wing flapping, several key frames are selected at the corresponding time points marked in Figure 3(a) ( $P_A$  to  $P_H$ ).

The time frame  $P_A$  and  $P_B$  are the time frames before and after the mid-downstroke. The leading edge vortex can be clearly seen at these two time frames (Figure 5(a) and Figure 5(b)). During this period, the lift coefficient keeps increasing along with the geometrical angle of attack until the stall angle is reached at  $62^\circ$ , where the delayed stall is stopped.

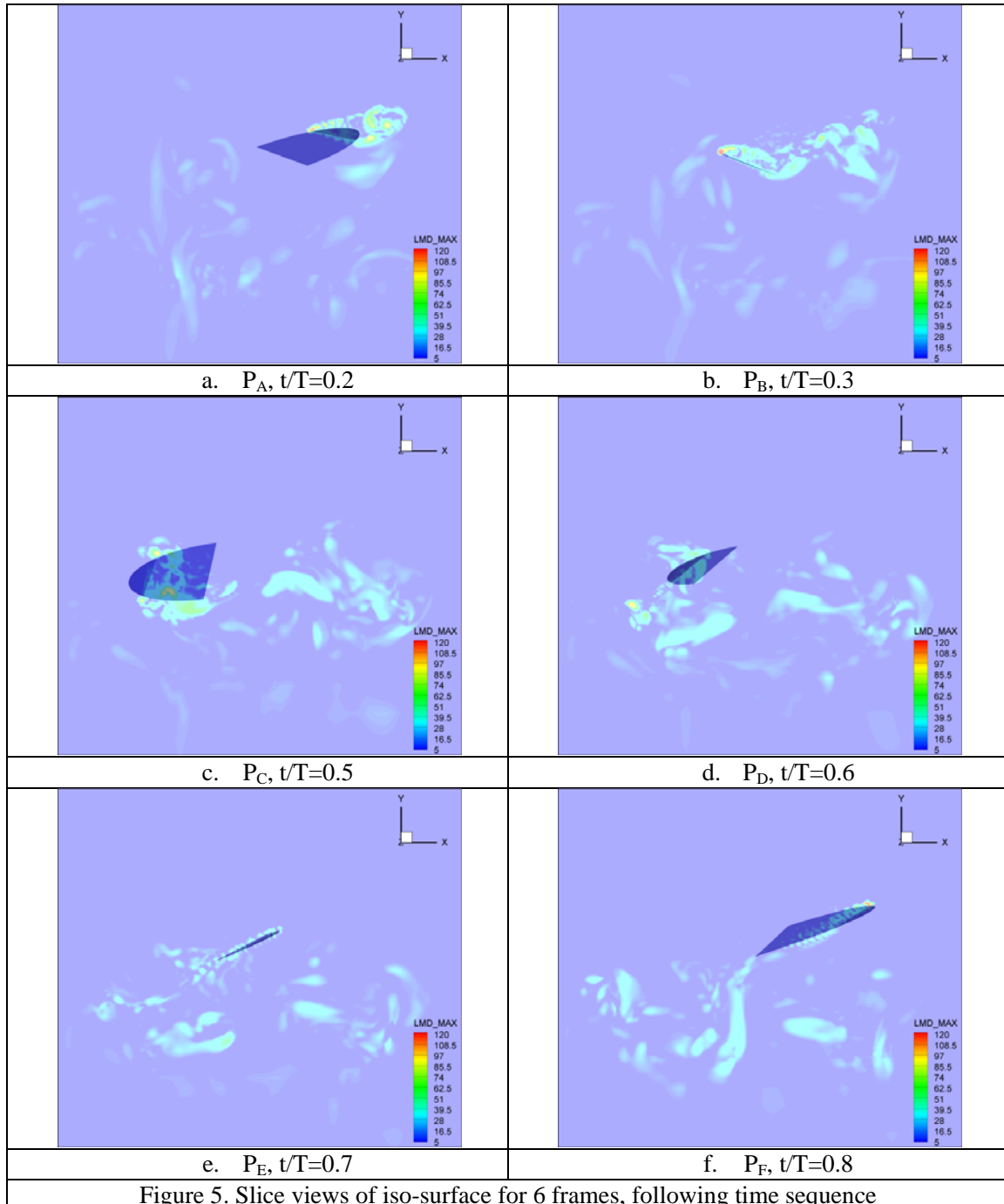
The frame  $P_C$  is the inflection point from downstroke to upstroke. After this point, the wing starts to move upward and the shed trailing edge vortex can be seen at  $P_D$ . Meanwhile, the strength of the leading edge vortex is weakened and totally diminishes at  $P_E$ . This agrees with the observation in Warrick et al. The frame  $P_F$  ( $t/T=0.8$ ) is right after the mid-upstroke. The leading edge vortex begins to form again due to the increase of the geometrical angle of attack. As a result, lift coefficient begins to increase in the upstroke.

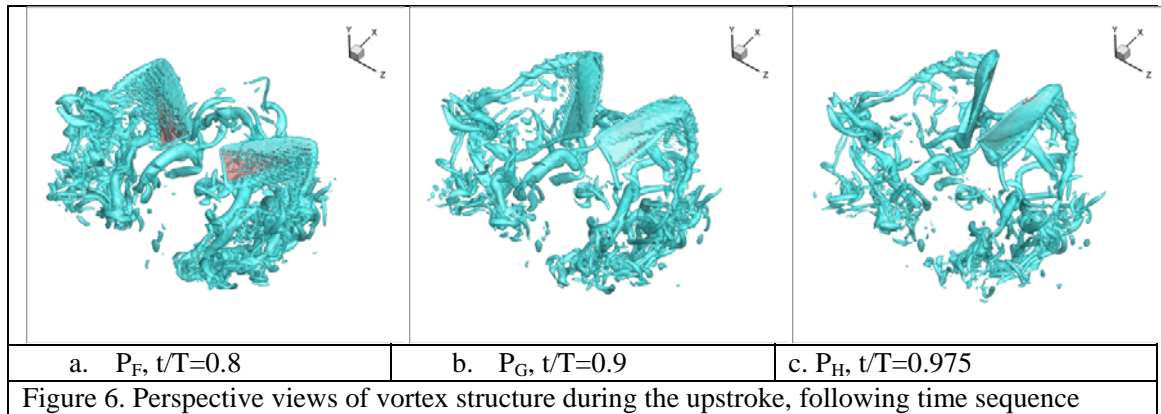
The wing begins the reversal rotation again at  $P_F$ . This causes local minimum point between  $P_F$  and  $P_G$  in the lift coefficient curve as shown in Figure 3(a). The continuously enhancing leading edge vortex delayed the stall (Figure 6) but finally the stall dominates the tendency of the curve until the wings are almost perpendicular in laboratory coordinate system and next downstroke is about to begin.

## Summary

A direct numerical simulation has been conducted to investigate wake structures of hummingbird hovering flight and associated aerodynamic performance. It's found that the amount

of lift produced during downstroke is about 2.95 times of that produced in upstroke. Two parallel vortex rings are formed at the end of the upstrokes. There is no obvious leading edge vortex can be observed at the beginning of the upstroke. Results are in good agreement with PIV experiments in Warrick et al. 2005 and Altshuler et al. 2009.





## Acknowledgement

This work is supported under DAGSI Student Fellowship and Wright State University Research Challenge grant.

## References

- <sup>1</sup>Altshuler D. L., Dudley, R., and Ellington, C. P., (2004), Aerodynamic forces of revolving hummingbird wings and wing models, *J. Zool., Lond.* 264, 327–332
- <sup>2</sup>Altshuler D. L., Princevac M., Pan H., Lozano J., (2009), Wake patterns of the wings and tail of hovering hummingbirds, *Exp Fluids* 46:835–846
- <sup>3</sup>Aono, H., Liang, F. and Liu, H. (2007). Near- and far-field aerodynamics in insect hovering flight: an integrated computational study. *J. Exp. Biol.* 211, 239-257.
- <sup>4</sup>Azuma, A., (2006), “The Biokinetics of Flying and Swimming”, Published by AIAA
- <sup>5</sup>Dickinson, M.H., Lehman, F. O. and Sane, S.P. (1999) Wing rotation and the aerodynamic basis of insect flight, *Science*, 284(5618): 1954-1960.
- <sup>6</sup>Dong, H., Mittal, R., and Najjar, F., 2006 Wake Topology and Hydrodynamic Performance of Low Aspect-Ratio Flapping Foils, *Journal of Fluid Mechanics*, 566:309-343, 2006.
- <sup>7</sup>Ellington, C. P. (1984), The Aerodynamics of Hovering Insect Flight. IV. Aerodynamic Mechanisms. *Phil. Trans. R. Soc. Lond. B* Vol. 305, pp 79-113.
- <sup>8</sup>Ellington, C. P. (1999), The novel aerodynamics of insect flight: Applications to micro-air vehicles. *The Journal of Experimental Biology*. Vol. 202, pp 3439-3448.
- <sup>9</sup>Ellington, C. P., Van den Berg, C., Willmott, A. P., and Thomas, A. L. R. (1996) Leading-edge vortices in insect flight. *Nature*, 384: 626-630.
- <sup>10</sup>Lehmann, F. O., Sane, S. P., and Dickinson, M. H. (2005), The aerodynamic effects wing-wing interaction in flapping insect wings, *Journal of Experimental Biology*, 208: 3075-3092.

- <sup>11</sup>Liang Z., Dong H., Wei M., 2009, Unsteady Aerodynamics and Wing Kinematics Effect in Hovering Insect Flight, *AIAA-2009-1299*
- <sup>12</sup>Mittal, R., Dong, H., Bozkurttas, M., Najjar, F. M., Vargas, A., and von Loebbecke A., (2008), A versatile sharp interface immersed boundary method for incompressible flows with complex boundaries, *Journal of Computational Physics*, 227:4825-4852.
- <sup>13</sup>Poelma C., Dickson, W.B. and Dickinson, M. H. (2006), Time-resolved reconstruction of the full velocity field around a dynamically-scaled flapping wing, *Experiments in Fluids*, 41: 213-225.
- <sup>14</sup>Sane, S. P., Dickinson, M. H., (2001), The control of flight force by a flapping wing: lift and drag production, *The Journal of Experimental Biology* 204, 2607-2626.
- <sup>15</sup>Taylor, G. K., Nudds, R. L., and Thomas, A. L. R., 2003, Flying and swimming animals cruise at a Strouhal number tuned for high power efficiency, *Nature* Vol. 425.
- <sup>16</sup>Tobalske B. W., Warrick D. R., Clark C. J., Powers D. R., Hedrick T. L., Hyder G. A. and Biewener A. A., 2007, Three-dimensional kinematics of hummingbird flight, *The Journal of Experimental Biology* 210, 2368-2382
- <sup>17</sup>Warrick, D. R., Tobalske, B. W., and Powers, D. R. (2005) "Aerodynamics of the hovering hummingbird", *Nature*, Vol. 435, No. 23, pp. 1094-1097.
- <sup>18</sup>Weis-Fogh, T. (1972). Energetics of Hovering Flight in Hummingbirds and in *Drosophila*. *J. Exp. Biol.* 56, 79-104.
- <sup>19</sup>Weis-Fogh, T. (1973). Quick estimates of flight fitness in hovering animals, including novel mechanisms for lift production. *J. Exp. Biol.* 59, 169-230.